Remediation of water containing mercury(II) using poly 2-aminothiazole intercalated α-zirconium phosphate nanoplates

Saadia M. Waly[1], Ahmad M. El-Wakil[1], Weam M. Abou El-Maaty[1], and Fathi S. Awad[1,2*]

[1]Chemistry Department, Faculty of Science, Mansoura University, Mansoura 35516, Egypt.
[2] Chemistry Department, Faculty of Science, New Mansoura University, New Mansoura 35712, Egypt.

Supporting Information

S1: Characterization

The ZrP nanoplates and AT@ZrP nanocomposite were characterized using a diversity of analytical techniques. Fourier transform infrared (FTIR) spectra were recorded using a Nicolet-Nexus 670 spectrometer equipped with a diamond ATR accessory. The measurement employed a resolution of 4 cm^{-1} and 32 scans. The crystal structure of the sample was analyzed using powder X-ray diffraction (XRD) on a PANalytical MPD X'Pert PRO diffractometer. The measurements employed 45 kV, 40 mA Ni-filtered Cu Kα1 radiation at room temperature. X-ray photoelectron spectra (XPS) were obtained on a Thermo-Fisher ESCALAB 250 spectrometer equipped with a micro-focused, monochromated Al Kα X-ray source operating at 15 kV and a double-focusing, full 180° spherical sector electron analyzer. Scanning electron microscopy (SEM): A Hitachi SU-70 field-SEM with an energy of 5.0 kV was used to take the SEM images. Transmission electron microscopy (TEM): A JEOL JEM1400 TEM was used to obtain the TEM images at 100 kV.

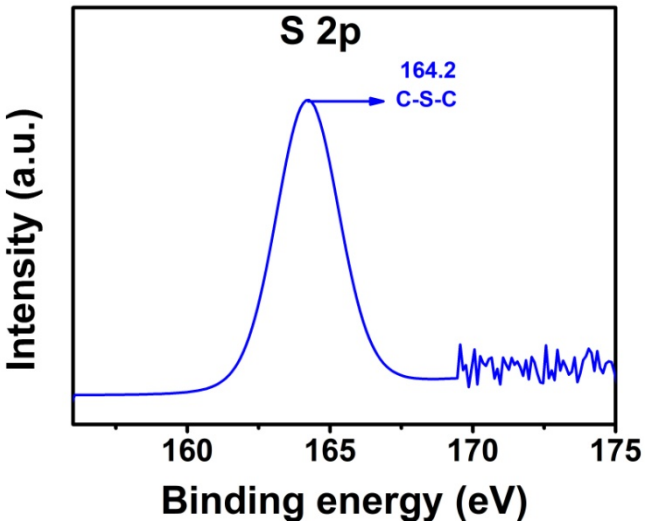

Figure S1: High XPS resolution of S 2p.

S2. Determination of Point of Zero Charge (pH_{PZC})

To determine the pH_{PZC}, a series of solutions with pH values ranging from 2 to 12 were prepared by adjusting the pH of 0.01 M NaCl solutions using 0.1 M NaOH or 0.1 M HCl. Each solution (50 mL) was placed in an Erlenmeyer flask, and 0.15 g of the adsorbent was added. The flasks were then shaken for 48 hours to ensure equilibrium. The final pH of each solution was measured and compared to the initial pH. The pH_{PZC} was determined as the point where the curve of pH_{final} versus $pH_{initial}$ intersected the line where $pH_{final} = pH_{iniial}$.

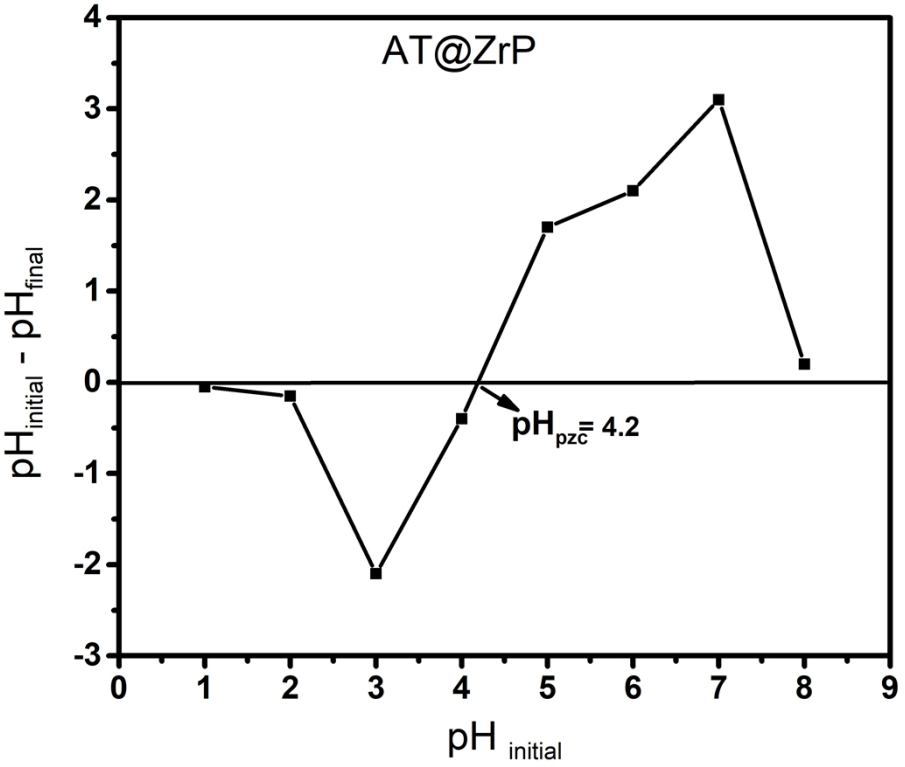

Figure S2: Determination of pH_{pzc} of AT@ZrP

S3.

The Langmuir and Freundlich isotherm models are two extensively used mathematical models. The Langmuir model assumes a monolayer coverage and that all the adsorbent sorption sites are the same while the Freundlich isotherm model assumes that the coverage is multilayer and that all the adsorption sites are heterogenous. The Langmuir and Freundlich models are presented as Eq.(1) and Eq. [2], respectively, as follows:[1-2]

$$\ln q_e = lnK_f + \frac{1}{n} lnC_e \quad (1)$$

$$\frac{C_e}{q_e} = \frac{1}{b\,Q_0} + \frac{C_e}{Q_0} \quad (2)$$

Where q_e, C_e, b, and Q_o are the equilibrium adsorption capacity, the equilibrium concentration of the metal ions, the Langmuir constant, and the Langmuir monolayer adsorption capacity, respectively. 1/n and K_f are the adsorption intensity and the Freundlich constant, respectively.
Moreover, the essential feature of the Langmuir isotherm can be defined as RL parameter given by **Eq. (3)**.[3]

$$R_L = \frac{1}{1 + bc_0} \qquad (3)$$

The separation factor (R_L) can be used to indicate the shape of the adsorption behavior to be either irreversible (R_L = 0), linear (R_L = 1), unfavorable (R_L> 1), or favorable (0 < R_L < 1).[4]

S4.
The PFO model usually predicts the behavior at the initial stage of the adsorption process, while PSO model predicts the behavior at all stages of the adsorption process[5].
Pseudo-first-order kinetic model:

$$\log(q_e - q_t) = \log q_e - \frac{K_1 t}{2.303} \qquad (4)$$

Pseudo-second-order kinetic model:

$$\frac{t}{q_t} = \frac{1}{K_2 q_e^{\,2}} + \frac{t}{q_e} \qquad (5)$$

Where k_1 (min^{-1}) and k_2 (g mol^{-1} min^{-1}) are the rate constants. q_t and q_e are the adsorption uptake of heavy metal at time t (min) and at equilibrium. Where k_1 (min^{-1}) and k_2 (g mol^{-1} min^{-1}) are the rate constants. q_t and q_e are the adsorption uptake of heavy metal at time t (min) and at equilibrium.

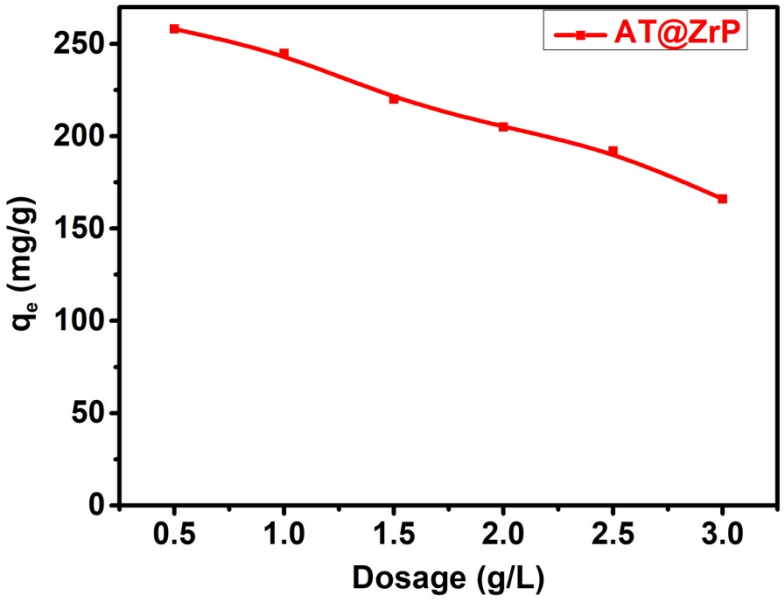

Figure S3: Effect of adsorbent dosage on the maximum adsorption capacity of Hg(II) using AT@ZrP.

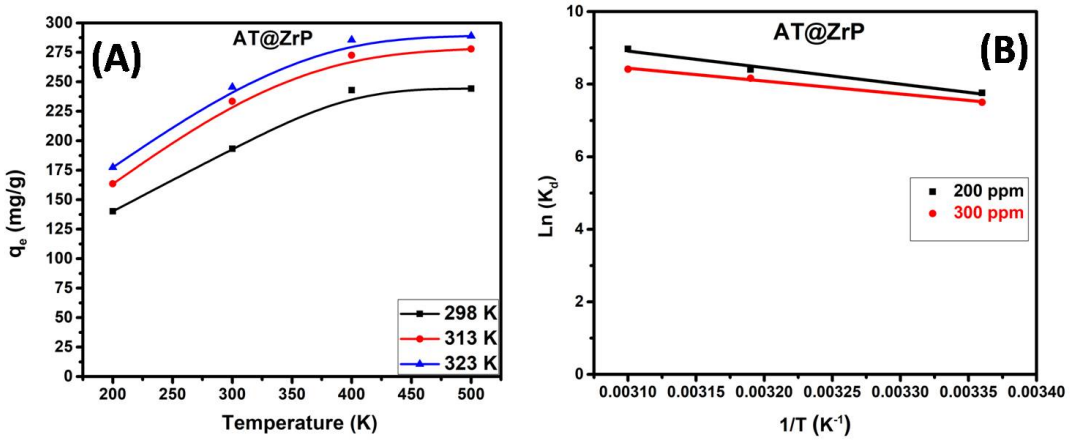

Figure S4: (A) The adsorption capacity of AT@ZrP as a function of temperature; (B) The plots of $\ln K_d$ versus T^{-1} for estimations of thermodynamic parameters of the adsorption process of Hg(II) on AT@ZrP.

Table S1. Thermodynamic parameters for the adsorption of Hg(II) onto AT@ZrP at different temperatures.

Metal concentration (mg/L)	ΔH°(kJ/mol)	ΔS°(kJ/mol)	ΔG°(kJ/mol)		
			298K	313K	323K
200.0	82.77	0.35	-21.53	-26.88	-30.38
300.0	80.28	0.33	-18.06	-23.01	-26.31

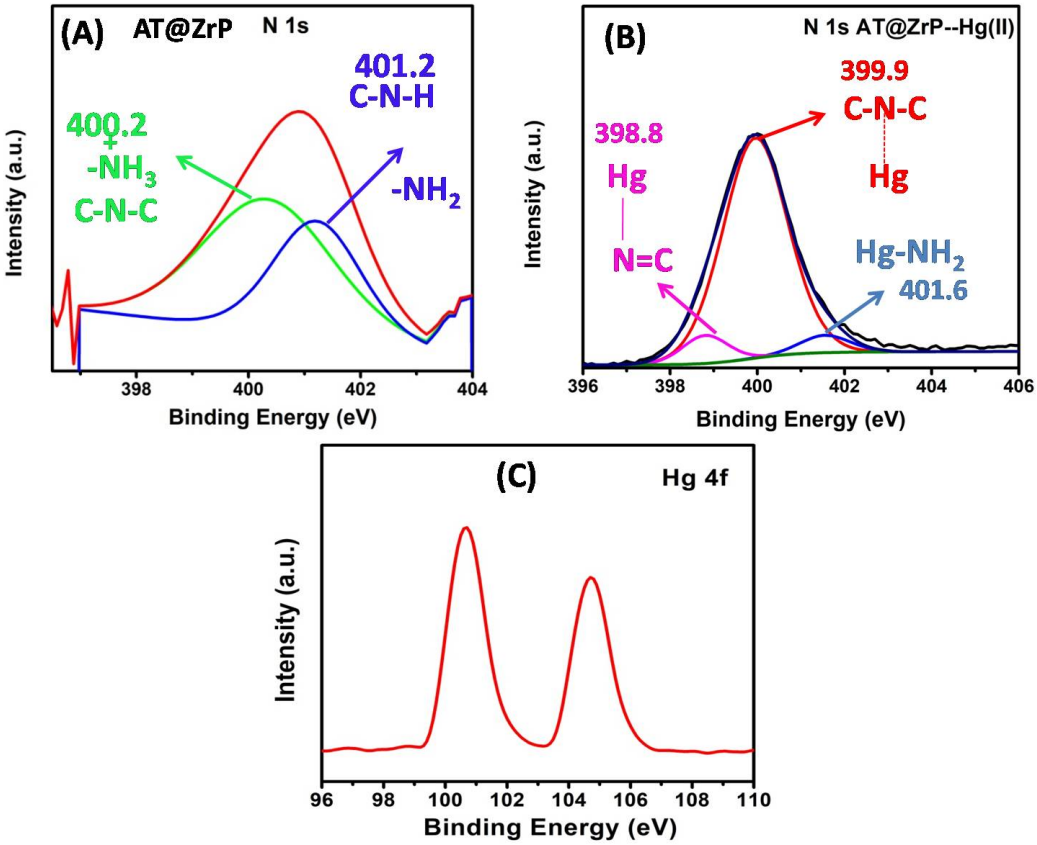

.

Figure S5: High XPS resolution of N 1s in AT@ZrP before adsorption (A), N 1s in AT@ZrP after Hg(II) adsorption, and Hg 4f in AT@@ZrP after Hg(II) adsorption.

References

1. F. S. Awad, K. M. AbouZied, W. M. Abou El-Maaty, A. M. El-Wakil and M. S. El-Shall, *Arabian Journal of Chemistry*, 2020, **13**, 2659-2670.
2. S. Pourbeyram, *Industrial & Engineering Chemistry Research*, 2016, **55**, 5608-5617.
3. F. A. Pavan, A. C. Mazzocato and Y. Gushikem, *Bioresource technology*, 2008, **99**, 3162-3165.
4. M. S. Alhumaimess, *Separation Science and Technology*, 2020, **55**, 1303-1316.
5. A. M. El-Wakil, S. M. Waly, W. M. Abou El-Maaty, M. M. Waly, M. Yılmaz and F. S. Awad, *ACS omega*, 2022, **7**, 6058-6069.